Applied Physics Letters ARTICLE scitation.org/journal/apl

Telecom InP-based quantum dash photodetectors grown on Si

Cite as: Appl. Phys. Lett. **118**, 141101 (2021); doi: 10.1063/5.0045485
Submitted: 26 January 2021 · Accepted: 24 March 2021 ·
Published Online: 7 April 2021

Ying Xue,[1] Yi Wang,[2] Wei Luo,[1] Jie Huang,[1] Liying Lin,[1] Hon Ki Tsang,[2] and Kei May Lau[1,a)]

AFFILIATIONS

[1]Department of Electronic and Computer Engineering, Hong Kong University of Science and Technology, Hong Kong, China
[2]Department of Electronic Engineering, The Chinese University of Hong Kong, Hong Kong, China

[a)]Author to whom correspondence should be addressed: eekmlau@ust.hk. **Tel.:** (852)23587049. **Fax:** (852) 23581485

ABSTRACT

Photodetectors on Si with high responsivity, large bandwidth, and multispectral operation are required for high data rate communications using Si photonics. We report characteristics of InP-based quantum dash (QDash) photodetectors with a p-i-n structure directly grown on (001) Si. Three layers of quantum dashes were grown on InP on Si templates and fabricated into waveguide photodetectors. The QDash photodetectors can operate from 1240 nm to 1640 nm, covering the entire telecommunication band. A low dark current density of 2.1×10^{-6} A/cm^2, responsivities of 0.35 ± 0.05 A/W at 1550 nm and 0.94 ± 0.05 A/W at 1310 nm, and a 3-dB bandwidth of 10.3 GHz were demonstrated. Our results show that the QDash photodetectors grown on Si hold great potential for on-chip integration in Si-photonics.

Deployment of Si-photonics is driven by the unprecedented rapid growth in the demand of high-volume and high-speed data communications. Leveraging the complementary metal-oxide-semiconductor (CMOS) technology of the microelectronics industry, Si photonics is now widely accepted as a platform for photonic integration in high capacity data communications because of its large bandwidth, scalable high-yield manufacturing, and low cost.[1,2] In the photonic toolbox, Si-based passive components such as the low loss waveguide,[3] high-efficiency grating coupler,[4] and high-speed modulator have witnessed tremendous progress.[5] However, light emission and detection still rely on non-Si material.[6] Ge photodetectors (PDs) on Si are routinely offered by commercial foundries because of their compatibility with CMOS technology.[7,8] Although waveguide-integrated Ge on Si PD can offer high responsivity within the 1550 nm band, its inherent high dark current introduces shot noise, which limits its sensitivity at high frequency.[9,10] III–V photodetectors can be a promising alternative because they can offer lower dark current in the telecom band,[11] and the monolithic integration of III–V photodetectors on Si can potentially provide a better solution for light detection in Si-photonics. Specifically, III–V quantum structures with three-dimensional confinement such as quantum dots (QDs) and quantum dashes (QDashes) emerge as superior active media for optical devices grown on Si, benefitting from their excellent high temperature stability and less sensitivity to crystal defects.[12] Taking the advantages of high-quality III-V epitaxy on Si and the tight confinement of quantum structures, advances have been reported on lasers and photodetectors, with works mostly focused on the GaAs-based material system operating in the O band.[13–15] However, for the C band, which is crucial for long-haul communications, there are only limited reports due to the challenge of extending the wavelength in the GaAs-based material system.[16,17] Compared with GaAs, InP-based optical devices can be applied in both the O band and the C band.[18] Additionally, they can leverage on the device technologies developed for photonic integrated circuits on InP, thereby benefitting the future photonic integration on Si.

Here, we present the InP-based InAs/InGaAs/InAlGaAs QDash photodetectors grown on nominal (001) Si covering the entire telecom band. The fabricated QDash photodetector features external (relative to incident power from the optical fiber) responsivities of 0.35 ± 0.05 A/W at 1550 nm and 0.94 ± 0.05 A/W at 1310 nm with a wavelength detection range over 400 nm. A low dark current of 42 pA at –1 V bias was measured, which corresponds to a current density of 2.1×10^{-6} A/cm^2. A 3-dB bandwidth of 10.3 GHz was demonstrated by the impulse response measurement. This value may be further improved by shrinking the dimension of the photodiode. The photodetector was also analyzed by calculating the specific detectivity and the noise equivalent power (NEP). A specific detectivity of around 5.7×10^{10} cm Hz$^{1/2}$/W and an NEP of around 7.8×10^{-14} W/Hz$^{1/2}$ was achieved. The InP-based photodetectors leverage the same epitaxial structure with QDash lasers,[19] suggesting potential integration of the photodetectors and lasers on a single chip. These results mark an important step toward the monolithic integration of high-performance photodetectors on Si.

The growth structure of the QDash photodetector and the atomic force microscope (AFM) photo of the QDashes with an estimated density of $3 \times 10^{10}\,\text{cm}^{-2}$ are schematically illustrated in Fig. 1(a). The p-i-n photodiode was grown on an optimized InP on a planar Si (IoPS) template. The IoPS template consists of 1.1 μm of GaAs directly grown on planar Si and 3.1 μm of InP buffer grown on GaAs on Si. GaAs grown on Si by thermal cycle annealing (TCA) provides an anti-phase boundary (APB)-free growth front for the following InP growth. Hence, smooth InP buffer on Si was achieved. The top surface roughness, as measured by AFM, was about 3 nm. The threading dislocation density measured after the InP buffer growth is around $3.6 \times 10^8/\text{cm}^2$. Thick upper and lower cladding layers were applied for better optical confinement, which will help improve the responsivity. A three-layer InAs/InGaAs dash-in-well structure embedded in InAlGaAs cladding was grown on the high-quality InP as the absorption layer. P-doped InGaAs and n-doped InP with doping levels of $1.6 \times 10^{19}\,\text{cm}^{-3}$ and $5 \times 10^{18}\,\text{cm}^{-3}$, respectively, were grown as contact layers for applying the electrical bias. The QDash growth was optimized according to the photoluminescence (PL) performance to ensure the high-quality QDash that is crucial for realizing the low dark current and high photo-response of the photodetector. The room temperature PL of the optimized three-layer QDashes grown on Si without the thick cladding and contact layers is presented in Fig. 1(b). The entire growth was performed in our metalorganic chemical vapor deposition (MOCVD) system, with growth details and characterization, as well as comparison of the QDashes grown on Si and InP substrates reported in Refs. 19 and 20. The as-grown sample was fabricated into waveguide p-i-n photodetectors using conventional photolithography, dry etch, and metallization steps. A passivation layer of 600 nm-thick oxide was deposited to suppress the dark current. Ti/Pt/Au (400/400/1200 nm) and Ge/Au/Ni/Au (400/400/240/1000 nm) were evaporated for the p- and n-contact metals, respectively. Figure 1(c) displays the cross-sectional scanning electron microscope (SEM) image of the finished device with a ridge width of 4 μm. The mirror-like end facets enable low coupling loss between the excitation light and the photodetector under test.

The QDash photodetector was first characterized by current-voltage (*I-V*) measurements without light illumination. The dark current of the QDash photodetector with a width of 4 μm and a length of 500 μm is presented in Fig. 2(a). Recently, dark current densities of 1.3×10^{-4} A/cm^2 at –1 V for GaAs-based QD photodetectors grown on GaP/Si and 1×10^{-6} A/cm^2 at –1 V for GaAs-based QD photodetectors bonded on Si were reported.[21,22] For our photodetector, a low dark current of 42 pA was measured at -1 V, which corresponds to a low dark current density of 2.1×10^{-6} A/cm^2. At a bias of –2 V, the dark current increased to 193 pA, corresponding to a current density of 9.6×10^{-6} A/cm^2. To measure the photoresponse, the QDash photodetector was illuminated by both a C band and an O band tunable laser. The excitation light from the laser was butt coupled into the photodetector using a lensed fiber with a spot size of around 4 μm. The photo-current was collected and measured using a source meter. The *I-V* curves for the 4 μm wide, 500 μm long device under illumination are shown in Fig. 2(b). With an incident power of around 11 μW, photocurrents of 10 and 4 μA were measured at 1310 and 1550 nm, respectively. The corresponding responsivity was calculated relative to the optical power in the incident optical fiber and plotted as a function of applied bias in Fig. 2(c). The responsivity at 1550 nm remains at 0.35 ± 0.05 A/W when the bias sweeps from –6 V to 0 V. The external quantum efficiency (EQE) at 1550 nm was calculated to be 28% using $0.35 \times 1.24/1.55$. The responsivity at 1310 nm was extracted to be 0.94 ± 0.05 A/W, which is 2.5 times that at 1550 nm. This might be a result of the higher absorption coefficient of the InAs QDash layer at 1310 nm.[23] The high responsivity could benefit from the 500 μm long PD waveguide, which maximizes light absorption as reported in other waveguide PDs.[24,25] Similar to the photoresponse measured at 1550 nm, the responsivity at 1310 nm shows no obvious dependence on the bias. The responsivity was achieved with only three layers of QDashes as the absorption layer and can certainly be improved by increasing the number of QDash layers.

We also investigated the power dependence of the photocurrent. The photocurrent measured under elevated optical power is depicted in Fig. 3(a) with a log-log representation. The linear line of the data indicates that the photocurrent and incident power follow well with the power law:

$$I_{ph} = A \cdot P^{\alpha},$$

where I_{ph} is the photocurrent, A is a parameter related to responsivity, P represents the excitation laser power density, and α is a fitting exponent of the power law. By fitting the data points in Fig. 3(a), an α value of 1 can be extracted, which means that the photocurrent is linear with

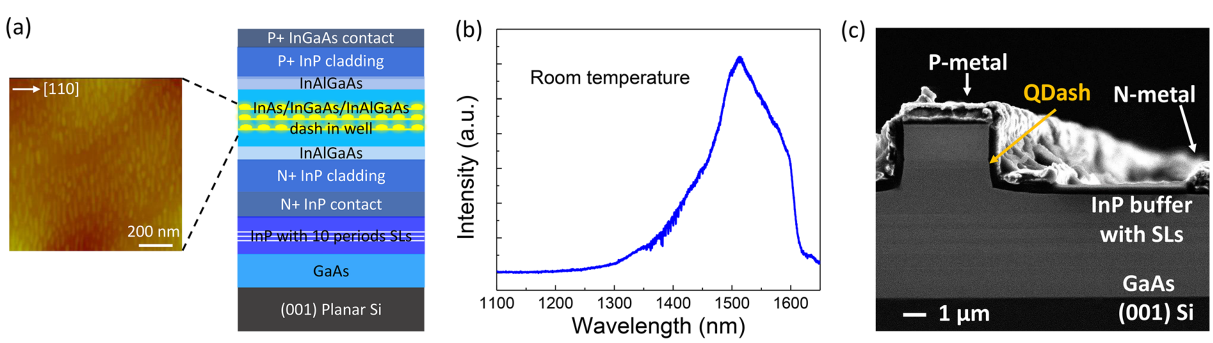

FIG. 1. (a) Schematic showing the epitaxial structure of the QDash photodetector and AFM photo of as-grown QDashes. (b) Room temperature PL of the three layers of QDashes grown on Si without cladding the contact layers. (c) Cross-sectional SEM image of a fabricated waveguide photodetector with a ridge width of 4 μm.

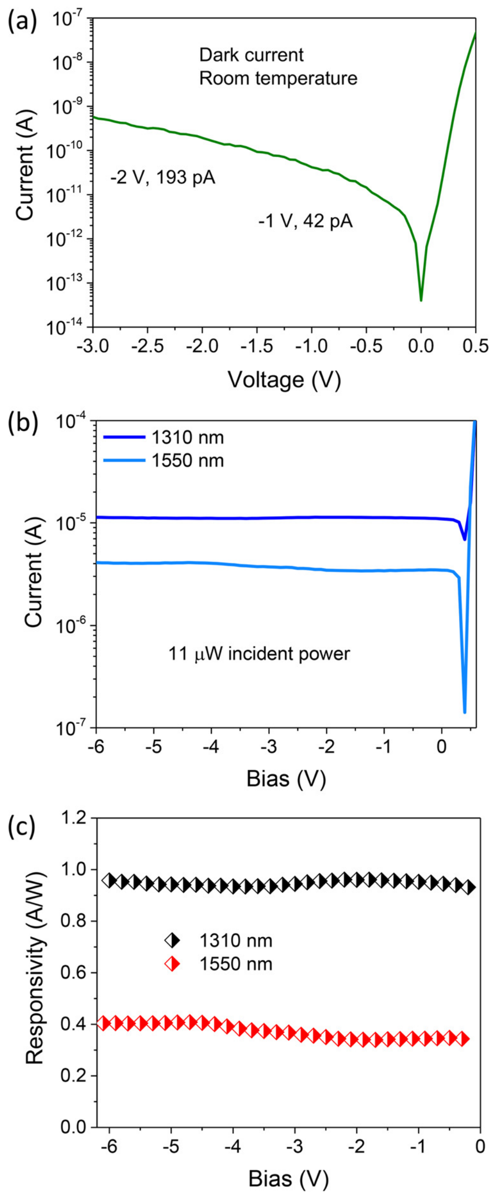

FIG. 2. (a) *I-V* curve on the log scale without light illumination for the 4 μm wide, 500 μm long device. (b) *I-V* curves measured at 1310 and 1550 nm at an incident power of 11 μW. (c) Responsivity at 1310 and 1550 nm as a function of an applied bias from -6 V to 0 V.

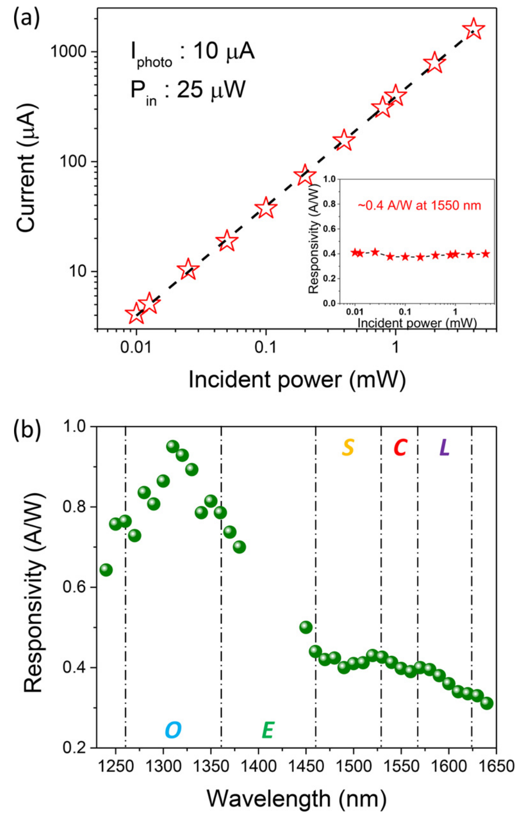

FIG. 3. (a) Measured current plotted vs incident power on the log-log scale, inset: responsivity extracted at various excitation powers. (b) Responsivity distribution at various wavelengths between 1240 and 1640 nm.

the incident power. As a result, the responsivity at different incident powers maintains a constant value of around 0.4 A/W, as presented in the inset of Fig. 3(a), indicating that our photodetector is nearly trap-free.[26] Benefiting from the high efficiency of the QDashes, the photodetector is ultrasensitive, as exemplified by the measured photocurrent of ~40 nA when the illuminating optical power was decreased to180 nW (detection limitation of the power meter in the test setup). The operation wavelength of the photodetector was studied by measuring the photocurrent at various wavelengths from 1240 nm to 1640 nm under identical incident power. The responsivities measured at different wavelengths are shown in Fig. 3(b). With the expansion of the operating wavelength, the responsivity peaked to 0.94 A/W at 1.3 μm and then gradually declined to 0.31 A/W until it reached 1640 nm. The missing data between 1380 and 1450 nm were due to the limitation of the laser tuning range. The responsivity in this range can be inferred by the data at the shorter and longer wavelengths. We believe that the PD covers an operation wavelength range exceeding 400 nm, covering the O, E, S, C, and L band.

Having a high speed response is essential for photodetectors used in high-speed data communications. We studied the 3-dB bandwidth of our photodetector by carrying out impulse-response measurements with the test setup depicted in Fig. 4(a).[27] A pulse from a 1550 nm mode-lock fiber laser with a full width at half maximum (FWHM) of 100 fs was coupled into the QDash photodetector. Then, the output electrical pulse generated by our photodetector was observed on a 60-GHz-bandwidth sampling oscilloscope. The variable optical attenuator and power meter were placed for power adjustment and monitoring. The output pulses from the photodetector at –1 V, –3 V, and –5 V biases are shown in Fig. 4(b). The pulse width shows a clear dependence on the bias. The impulse response at –5 V demonstrates an FWHM of 43 ps. The 3-dB bandwidth is calculated to be 10.3 GHz using the time-bandwidth product of $\Delta f \cdot \Delta t = 0.441$, where Δf is the 3-dB bandwidth of the photodetector and Δt is the FWHM of the

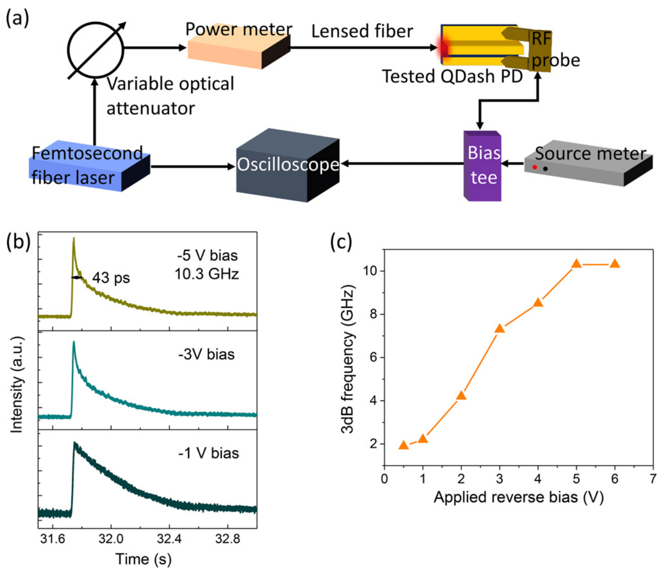

FIG. 4. (a) Illustration of the test setup for the impulse-response measurement. (b) Impulse-response measurement results at bias voltages of –1, –3, and –5 V with an extracted 3-dB bandwidth of 10.3 GHz at –5 V. (c) Evolution of the 3-dB bandwidth with the increase in reverse bias.

output pulse.[28] This value may be further enhanced by reducing the device dimensions. During the measurement, the FWHM of the impulse response first decreased with the increase in the reverse bias and then remained constant for bias higher than 5 V. The change in the 3-dB bandwidth with bias is displayed in Fig. 4(c). The larger 3-dB bandwidth at higher reverse bias can be attributed to the reduced carrier transient time.[29] Detectivity is also an important figure of merit for a photodetector, and specific detectivities of 6.5699×10^8 cm Hz$^{1/2}$/W and 3.77×10^9 cm Hz$^{1/2}$/W were reported for the GeSn/Ge photodetector grown on Si and the QD photodetector bonded on Si, respectively.[30–32] We analyzed our photodetector performance by calculating the specific detectivity D^* and the NEP. The specific detectivity is calculated as follows:[33]

$$D^* = R(\lambda)\sqrt{\frac{A}{2qI_{dark}}},$$

where $R(\lambda)$ is the responsivity, A is the junction area, q is the elementary charge, and I_{dark} is the dark current. Due to the low dark current, a high specific detectivity of around 5.7×10^{10} cm Hz$^{1/2}$/W was achieved at 1550 nm. Then, we also estimated the NEP of the QDash photodetector by only considering the shot noise and the Johnson noise using the following equation:[34]

$$NEP = \frac{\sqrt{2qI_{dark} + \frac{4k_BT}{R_d}}}{R(\lambda)},$$

where k_B is the Boltzmann constant, T is the temperature (300 K), and R_d is the resistance of the photodetector. The estimated NEP is $\sim 7.8 \times 10^{-14}$ W/Hz$^{1/2}$. This value together with the calculated specific detectivity agrees well with the relationship of $D^* = \frac{\sqrt{A}}{NEP}$.[35]

Ge photodetectors on Si with a 3-dB bandwidth of 10, 32, 42.5, and 70 GHz have been reported in the literature. However, their dark current is several orders of magnitude higher than those of the QD/QDash photodetector on Si. The lowest dark current density reported for the Ge photodetector on Si is 1×10^{-3} A/cm^2.[36–40] Our InP-based QDash photodetector demonstrated capability of operating in both the O band and the C band with high responsivity. 0.35 ± 0.05 A/W at 1550 nm and 0.94 ± 0.05 A/W at 1310 nm and the 10.3 GHz 3-dB bandwidth are among the highest for the QD/QDash photodetector grown both on Si and the native substrate.[21,22,41] Furthermore, this performance may be further improved by fine tuning the active region structure (such as improve homogeneity of the QDashes) and shrinking the device size. The high efficiency, large bandwidth, low dark current, and wide operation wavelength range of our photodetector support QDash being a promising active material for photodetectors on Si.

In conclusion, we demonstrated an InP-based QDash photodetector monolithically grown on Si. The photodetector can operate in the entire telecom band, spanning from 1240 nm to 1640 nm. A low dark current density of 2×10^{-6} A/cm^2, high responsivities of 0.35 ± 0.05 A/W at 1550 nm and 0.94 ± 0.05 A/W at 1310 nm, and a 3-dB bandwidth of 10.3 GHz are demonstrated. These performances together with the high detectivity, low NEP, and high sensitivity make it a superior candidate for on-chip detection in Si photonics. The photodetectors were grown on the same epitaxial structure and fabricated using a similar process to that of QDash lasers, which suggests the potential of integrating the photodetector and light source on a single chip for light detection in Si-photonics. With these results, this work provides a prospective solution toward realizing integrated photonic circuits on Si.

We acknowledge the Research Grants Council, University Grants Committee (Nos. 16212115 and 16245216), and Innovation and Technology Fund (No. ITS/273/16FP). The authors thank the NFF and MCPF of HKUST for technical support. Fruitful discussion with Dr. Yu Han is also acknowledged.

DATA AVAILABILITY

The data that support the findings of this study are available from the corresponding author upon reasonable request.

REFERENCES

[1] A. Ren, L. Yuan, H. Xu, J. Wu, and Z. Wang, J. Mater. Chem. C **7**(46), 14441–14453 (2019).
[2] Y. Han, Y. Xue, Z. Yan, and K. M. Lau, J. Lightwave Technol. **39**(4), 940–948 (2021).
[3] Z. Yu, A. Feng, X. Xi, and X. Sun, Opt. Lett. **44**(1), 77–80 (2019).
[4] Y. Tong, W. Zhou, X. Wu, and H. K. Tsang, Opt. Lett. **43**(23), 5709–5712 (2018).
[5] M. He, M. Xu, Y. Ren, J. Jian, Z. Ruan, Y. Xu, S. Gao, S. Sun, X. Wen, L. Zhou, and L. Liu, Nat. Photonics **13**(5), 359–364 (2019).
[6] Y. Geng, S. Feng, A. W. Poon, and K. M. Lau, IEEE J. Sel. Top. Quantum Electron. **20**(6), 36–42 (2014).
[7] S. Xu, W. Wang, Y. C. Huang, Y. Dong, S. Masudy-Panah, H. Wang, X. Gong, and Y. C. Yeo, Opt. Express **27**(4), 5798–5813 (2019).
[8] X. Lin, M. Natrella, J. Seddon, C. Graham, C. C. Renaud, M. Tang, J. Wu, H. Liu, and A. J. Seeds, Opt. Express **27**(25), 37065–37086 (2019).
[9] S. Lischke, D. Knoll, C. Mai, L. Zimmermann, A. Peczek, M. Kroh, A. Trusch, E. Krune, K. Voigt, and A. Mai, Opt. Express **23**(21), 27213–27220 (2015).

[10]D. Thomson, A. Zilkie, J. Bowers, T. Komljenovic, G. T. Reed, L. Vivien, D. Marris-Morini, E. Cassan, L. Virot, J. M. Fédéli, and J. M. Hartmann, J. Opt. **18**(7), 073003 (2016).
[11]A. Beling and J. C. Campbell, J. Lightwave Technol. **27**(3), 343–355 (2009).
[12]B. Shi, Y. Han, Q. Li, and K. M. Lau, IEEE J. Sel. Top. Quantum Electron. **25**(6), 1–11 (2019).
[13]J. Wu, Q. Jiang, S. Chen, M. Tang, Y. I. Mazur, Y. Maidaniuk, M. Benamara, M. P. Semtsiv, W. T. Masselink, K. A. Sablon, G. J. Salamo, and H. Liu, ACS Photonics **3**(5), 749–753 (2016).
[14]J. Huang, Y. Wan, D. Jung, J. Norman, C. Shang, Q. Li, K. M. Lau, A. C. Gossard, J. Bowers, and B. Chen, ACS Photonics **6**(5), 1100–1105 (2019).
[15]B. Chen, Y. Wan, Z. Xie, J. Huang, N. Zhang, C. Shang, J. Norman, Q. Li, Y. Tong, K. M. Lau, and A. C. Gossard, ACS Photonics **7**(2), 528–533 (2020).
[16]Y. Han, Z. Yan, W. K. Ng, Y. Xue, K. S. Wong, and K. M. Lau, Optica **7**(2), 148–153 (2020).
[17]S. Zhu, B. Shi, and K. M. Lau, Opt. Lett. **44**(18), 4566–4569 (2019).
[18]W. Luo, Y. Xue, B. Shi, S. Zhu, X. Dong, and K. M. Lau, Appl. Phys. Lett. **116**(14), 142106 (2020).
[19]Y. Xue, W. Luo, S. Zhu, L. Lin, B. Shi, and K. M. Lau, Opt. Express **28**(12), 18172–18179 (2020).
[20]W. Luo, Y. Xue, J. Huang, L. Lin, B. Shi, and K. M. Lau, Photonics Res. **8**(12), 1888–1894 (2020).
[21]Y. Wan, D. Jung, J. Norman, C. Shang, N. Nishiyama, S. Arai, A. C. Gossard, and J. Bowers, Appl. Phys. Lett. **113**(9), 093506 (2018).
[22]B. Tossoun, G. Kurczveil, C. Zhang, A. Descos, Z. Huang, A. Beling, J. C. Campbell, D. Liang, and R. G. Beausoleil, Optica **6**(10), 1277–1281 (2019).
[23]H. Chen, P. Verheyen, P. De Heyn, G. Lepage, J. De Coster, S. Balakrishnan, P. Absil, W. Yao, L. Shen, G. Roelkens, and J. Van Campenhout, Opt. Express **24**(5), 4622–4631 (2016).
[24]T. Yin, R. Cohen, M. M. Morse, G. Sarid, Y. Chetrit, D. Rubin, and M. J. Paniccia, Opt. Express **15**(21), 13965–13971 (2007).
[25]D. Ahn, C. Y. Hong, J. Liu, W. Giziewicz, M. Beals, L. C. Kimerling, J. Michel, J. Chen, and F. X. Kärtner, Opt. Express **15**(7), 3916–3921 (2007).
[26]Q. Zhao, W. Wang, F. Carrascoso-Plana, W. Jie, T. Wang, A. Castellanos-Gomez, and R. Frisenda, Mater. Horiz. **7**(1), 252–262 (2020).
[27]Y. Wang, Z. Yu, Z. Zhang, B. Sun, Y. Tong, J. B. Xu, X. Sun, and H. K. Tsang, ACS Photonics **7**(10), 2643–2649 (2020).
[28]A. Pospischil, M. Humer, M. M. Furchi, D. Bachmann, R. Guider, T. Fromherz, and T. Mueller, Nat. Photonics **7**(11), 892–896 (2013).
[29]X. Hu, D. Wu, H. Zhang, W. Li, D. Chen, L. Wang, X. Xiao, and S. Yu, Opt. Express **28**(25), 38343–38354 (2020).
[30]J. Szafraniec, S. Tsao, W. Zhang, H. Lim, M. Taguchi, A. A. Quivy, B. Movaghar, and M. Razeghi, Appl. Phys. Lett. **88**(12), 121102 (2006).
[31]H. Zhou, S. Xu, Y. Lin, Y. C. Huang, B. Son, Q. Chen, X. Guo, K. H. Lee, S. C. Goh, X. Gong, and C. S. Tan, Opt. Express **28**(7), 10280–10293 (2020).
[32]H. S. Kim, S. Y. Ahn, S. H. Kim, G. H. Ryu, J. H. Kyhm, K. W. Lee, J. H. Park, and W. J. Choi, Opt. Express **25**(15), 17562–17570 (2017).
[33]M. Shkir, M. T. Khan, I. M. Ashraf, A. Almohammedi, E. Dieguez, and S. AlFaify, Sci. Rep. **9**(1), 12436 (2019).
[34]Y. Wang, Z. Yu, Y. Tong, B. Sun, Z. Zhang, J. Xu, X. Sun, and H. K. Tsang, Appl. Phys. Lett. **116**(21), 211101 (2020).
[35]C. H. Ji, K. T. Kim, and S. Y. Oh, RSC Adv. **8**(15), 8302–8309 (2018).
[36]D. Feng, S. Liao, P. Dong, N. N. Feng, H. Liang, D. Zheng, C. C. Kung, J. Fong, R. Shafiiha, J. Cunningham, and A. V. Krishnamoorthy, Appl. Phys. Lett. **95**(26), 261105 (2009).
[37]L. Colace, G. Assanto, D. Fulgoni, and L. Nash, J. Lightwave Technol. **26**(16), 2954–2959 (2008).
[38]M. M. P. Fard, G. Cowan, and O. Liboiron-Ladouceur, Opt. Express **24**(24), 27738–27752 (2016).
[39]J. Liu, J. Michel, W. Giziewicz, D. Pan, K. Wada, D. D. Cannon, S. Jongthammanurak, D. T. Danielson, L. C. Kimerling, J. Chen, and F. Ö. Ilday, Appl. Phys. Lett. **87**(10), 103501 (2005).
[40]J. Michel, J. Liu, and L. C. Kimerling, Nat. Photonics **4**(8), 527—534 (2010).
[41]Y. Wan, C. Shang, J. Huang, Z. Xie, A. Jain, J. Norman, B. Chen, A. C. Gossard, and J. Bowers, ACS Nano **14**(3), 3519–3527 (2020).